Journal of University of Duhok, Vol.23, No.2 (Pure and Eng. Sciences),Pp 767-787, 2020 (Special Issue)
3rd international conference on recent innovations in engineering (ICRIE) Duhok, September 9-10-2020

PERFORMANCE OF RC SKEW BOX CULVERT: APPLICATION OF THE FINITE ELEMENT MODELLING AND ARTIFICIAL INTELLIGENCE

JAMES **H**. **H**AIDO[1*], **B**ASHAR **A**. **M**AHMOOD, **A**YAD **A**. **A**BDUL-**R**AZZAK[**], **M**ICHAEL **D**ORN[***] and **S**ALIM **T**. **Y**OUSIF [****]

[*]Dept. of Civil Engineering, College of Engineering, University of Duhok, Kurdistan Region-Iraq
[**]Dept. of Civil Engineering, College of Engineering, University of Mosul-Iraq
[***]Dept. of Building Technology, Linnaeus University-Sweden
[****]Al-Qalam University College, Karkuk-Iraq

(Accepted for Publication: December 29, 2020)

ABSTRACT

Box culvert structures are widely used nowadays in infrastructures such as roads or bridges worldwide. The skewness in the box culvert bridges is usually inevitable to achieve the desirable design of their layout. Based on the limited knowledge in proposing a simple mathematical model to predict the load-carrying capacity of these skew structures, more studies are regarded essential in this direction. The work presented is dealing with the modeling of the skewed reinforced concrete (RC) box culverts using a valid finite element modeling in ANSYS-11. In addition, artificial neural network (ANN) was adopted to formulate a mathematical model for the response of these bridges depending on the outputs of parametric study of the present finite element simulation. Specific nonlinear relationships have been employed in the numerical analysis to model the behavior of both concrete and embedded steel bars. A database of the performance of RC skew culverts, established from the outputs of over 285 finite element models, was utilized for the development of ANN-based models. The skew angle of the culvert, the span of its top slab, thickness of the slab and concrete compressive strength have been used as input variables to predict the behavior of the culvert via the developed ANN. Simple equations were derived depending on the results of this network to compute the failure load and maximum deflection of the top slab of the skew culvert. The proposed models showed superior efficiency over existing tedious analytical or numerical solution with consideration of combined effect of simplicity and accuracy in the output prediction. Moreover, the comparison of the finite element outcomes with those of previous experimental work confirms the validity of the used constitutive relationships in the analysis of single-cell concrete culverts.

KEYWORDS: reinforced concrete; Artificial Neural Network; box culvert structures; finite element simulation

1. INTRODUCTION

Box culverts are categorized as paramount transport infrastructures with high economical value [1]. These structures are mainly used in roadways, railways, sewerage conduits, storm runoff, waterways, pathways of telephone and electrical lines and stock or pedestrian underpass [2, 3]. A concrete culvert is the widely used type of culvert and is typically a reinforced concrete box [4] with rectangular cross sectional area [5]. The concrete of the box culverts can either be cast in situ or precast; recent technology indicates that the precast concrete is commonly used in culvert construction in the last decade [6]. The applied loadings of the concrete culverts, during their service life, are complex although they are built with single or multi cell box [7]. Typically, concrete box culverts are designed based on simplified behavior under loads and usually depend on considerable empiricism [8]. To understand the performance of reinforced concrete culverts and skewed concrete bridges, a series of analytical and experimental investigations have been performed. Chauhan et al. [9] examined the influence of skewness angle on the behavior of reinforced concrete bridge deck, with and without beams on the edge concrete beams, utilizing finite element modeling. Four nodes plate elements and two nodes beam elements were used to model the concrete slab and edge beam, respectively. Observations revealed that the skewness angle

james.haido@uod.ac; bashargxabd@gmail.com; ayadaghwan960@gmail.com
michael.dorn@lnu.se; salim.yousif@alqalam.edu.iq

has a remarkable effect on the abutment stiffness of the bridge. In addition, it is demonstrated that the deformation of the concrete deck slab decreases with increasing in the skewness angle of the bridge. The behavior of skewed precast concrete short span bridges with integral concrete abutments has been simulated by Zoghi et al. [10]; a parametric study has been carried out in this regard to show the effect of skewness. They concluded that the skewness of the bridge increases its bending moment capacity. Abuhajar et al. [8] investigated the interaction between the concrete box culvert and soil using a centrifuge physical model with small scale and considering the density and height of the soil above the box culvert. The measurements have been done for soil interaction factors and flexural moments of the culvert. These results proved that the soil culvert interaction factor is highly affected by the soil height above the culvert, the soil modulus of elasticity, the thickness of the culvert, as well as the Poisson's ratio of the soil. Design magnitudes of the static bending moments and static soil pressures for this structure were assessed using proposed equations and charts basing on the experimental results of the small scale model of the culvert. A numerical analysis was performed by Kim and Yoo [11] to study the effect of depth, width, stiffness and location of the compressible layer of the soil on the behavior of the deeply buried culvert. They found that the width of this layer should be less than 1.5 times the width of the culvert and the immediate placement of the compressible layer on the box culvert top will induce greatest reduction in the applied loading on the culvert. The evaluation of the applied earth pressure and its coefficient for the upper-buried culvert was carried out by Tao et al. [12] using a proposed numerical model. Accordingly, the equation of the coefficient of the soil arch was derived based on the measured earth pressure on the culvert via indoor model experiments with considering different heights of the soil filling. Calibration of the proposed model was performed by a comparison between numerical and experimental outcomes. Conclusions referred to that the slab thickness of the culvert sides, soil filling height and Poisson's ration and the proportion of the rock block are affected vividly by the earth pressure at the sides and top of the culvert. Moreover, analysis confirmed that there is a parabolic distribution of the vertical earth pressure on the top of culvert structure due to the shear lag influence. Yatsumoto et al. [13] worked on the centrifuge model experiments and numerical analysis of the buried box culverts. The validation of the analytical model was emphasized in the evaluation of bending moments for culverts with a square cross-sectional area. In addition, the analysis confirmed that there is high matching between analytical and experimental data in terms of shear deformation performance for these structures. Nevertheless, overestimation was found in the bending moment values of the culverts with wide cross sectional area. Bennett et al. [14] studied the behavior of a concrete box culvert with high embankments under vertical load. The width of this structure is less than the depth of the fill above its slab. The description of the results for an instrumented concrete culvert was given employing wall strain gauges, pressure cells and roof strain gauges. Noteworthy correlation was observed between the internal forces in the concrete culvert and height of fill, proposing that the factor of soil culvert interaction was independent on the ratio of the height of the soil above the roof of culvert (H) and its width (B). Furthermore, it was determined that the measured pressure on the culvert roof is markedly greater than the soil overburden pressure. Finite element analysis was used in the numerical analysis of deeply buried culverts by Kang et al. [15], taking into account the embankments' installation. The outputs showed that compacted and uncompacted sidefills of the culvert induce a frictional force that amounts averagely up to 78% and 80.5%, respectively, of the total applied vertical loading on the bottom side of the culvert. The results referred also to that the condition of the soil-culvert interface should be considered in the analysis to determine the design load of imperfect trench installation. McGuigan and Valsangkar [16] used a finite element technique in FLAC software to carry out a parametric study for the centrifuge testing of the box culvert with induced trenches installation. Conclusions were drawn on the unyielding and yielding foundations of the culverts. A finite element code was provided by Pimentel et al [17] to investigate the nonlinear performance of concrete box culvert with high embankment, considering the sequences in construction. The analysis indicated that the nonlinearity in the structural behavior is commenced when the height of the embankment ranged between 9.5 m

james.haido@uod.ac; bashargxabd@gmail.com; ayadaghwan960@gmail.com
michael.dorn@lnu.se; salim.yousif@alqalam.edu.iq

to 17.5 m. This is attributed to cracking onset in the culvert. Consequently, the stiffness of this structure decreased and got closer to the infill stiffness through the analysis. Yeom et al. [18] performed a study on the optimal joint positions to minimize the distresses of concrete pavement of skewed box culvert utilizing finite element simulation. The proved that lowest tensile stress of culvert top slab was reached when the joints were positioned over the culvert side directly for the case of straight culvert with skewness angle of 0^o. On the other hand, the minimum tensile stresses were determined in the roof of the skewed culvert when the joint is passing the intersection of the box culvert side and longitudinal axis of the top slab. The finite element modeling in SAP2000 software was adopted by Kumar and Ingle [19] to predict the behavior of skewed box underpass bridges. This parametric study pointed out that the height of the box has no influence on the response of this bridge. In spite of many endeavors in the direction of analysis of concrete box culverts, the structural engineering community has not yet comprehended the full complex performance of skew culverts due to large differences in both internal stresses within the culvert and its geometry. Thus, a reliable assessment approach for the behavior of the reinforced concrete skew bridges is regarded as an essential need to estimate the applied load capacity of these structures in a simplified manner. To this end, current study has been pursued at formulating a simple mathematical model appropriate for the structural assessment of reinforced concrete box skew box culverts using a new algorithm of analysis derived through the utilization of artificial neural network (ANN). This model is relied on the ability of an ANN-based approach to reach the closest conceivable fit to numerous data of the numerical analysis of concrete box culverts by finite element method using particular nonlinear models of concrete and steel bars behavior.

2. NUMERICAL MODELING WITH FINITE ELEMENTS

Finite element procedure in ANSYS was utilized to implement a structural analysis and a parametric study in order to compliment the behavior of single-cell reinforced concrete box culvert. The configurations of this structure tested previously under the incremental static loading were modelled with ANSYS using nonlinear constitutive models to simulate the performance of the material. Reinforced concrete is a nonhomogeneous composite material made of concrete and steel bar reinforcement. The mechanical characteristics of the concrete material change widely and cannot be easily examined due to the concrete heterogeneity. The investigation of the plastic performance of composite concrete materials is provided with utilizing constitutive relationships to predict the behavior of concrete under various loading cases. Nonlinear performance of concrete is attributed to cracking of concrete and crushing under the effect of tensile and compressive actions, respectively. Moreover, the interaction between concrete components as well as the slip between steel bars and concrete are inducing nonlinearity in the behavior of concrete structures. Finite element analysis is recommended to simulate the complicated response of concrete and consequently examine the cracking pattern and corresponding loading capacity of concrete members. Concrete has different resistances to compressive and tensile stresses. The behavior of this quasi-brittle material is usually investigated with finite element technique using various multi-linear or nonlinear models for stress-strain relationships. Nonlinear regression analysis has been performed in SPSS Statistics 22 to formulate a new mathematical relationship (Eq. 1) of the compressive stress values using previous experimental data [20, 21]; this model was used in the current finite element modeling. Remarkable matching was observed between the model predictions and the experimental data in terms of correlation coefficient (R^2) of 97.9%. The conditions of theory of plasticity are taken into account in establishing present nonlinear models between compressive stress and strain for concrete material.

$$\sigma_c = f'c \left({\varepsilon_c}/{\varepsilon}\right)^{-0.635} + 2.276 \qquad (1)$$

where,

σ_c = compressive stress in MPa

ε_c = compressive strain at the maximum stress

ε = compressive strain for the stress range of $0.3\, f'c$ - $f'c$

$f'c$ = compressive strength in MPa

Nonlinear performance of concrete under tension stresses starts in the post-cracking phase of concrete. The cracked concrete is able to stiffen the member in a phenomenon called

james.haido@uod.ac; bashargxabd@gmail.com; ayadaghwan960@gmail.com
michael.dorn@lnu.se; salim.yousif@alqalam.edu.iq

tension stiffening which depends on aggregate size, bar size, reinforcement ratio and crack width. In the current work, a multi-linear model (Fig. 1) was adopted to simulate the concrete behavior before and after cracking. The concrete shear retention factor was assumed to be 0.7 and 0.3 for closed and opened crack patterns of each finite element, respectively.

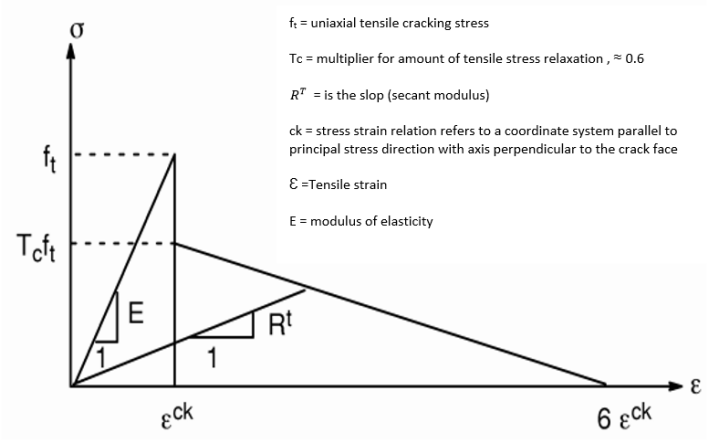

Fig. (1): Model of the tension behavior of concrete [22].

The behavior of steel bars and plates in tension and compression is similar and can be given in elastic-totally plastic stress-strain relationship [23] which is employed in the present finite element simulation.

Elements of type SOLID65 with eight nodes and three degrees of freedom at each node [22] were used in the modelling of the concrete parts. These solid elements are cracked and crushed under the effect of tensile and compressive stresses. Steel supports and bearing plates were modeled employing SOLID45 elements with similar nodes and degrees of freedom to SOLID65. Consequently, the applied load on the supports will distributed evenly with using SOLID45 to avoid the concentration of stresses which affects the convergence of solution. Concrete elements were defined with linear and multi-linear isotropic properties using the Willam and Warnke [22] model to predict the mode of failure.

The modelling of steel reinforcement was performed via LINK8 elements with uniaxial behavior under compressive and tensile loading; these elements have two nodes with three degrees of freedom per node [22].

3. VALIDATION OF THE FINITE ELEMENT MODELING

Finite element analysis comprising above-mentioned constitutive relationships was used to simulate the behavior of a reinforced concrete box culvert (Fig. 2) tested by Woo et al [24]. The finite element mesh has been formulated in ANSYS 11 using the aforementioned elements for concrete and steel bars as illustrated in Fig. 3. The validation of the present finite element procedure was examined by comparing the experimental observations with those for numerical analysis in terms of applied load-deflection curve and cracking pattern of the culvert. Fig. 4 reveals that there is a matching ratio of 90% between experimental and finite element results concerning load-carrying capacity and ultimate deflection at mid-span of the top slab of culvert. The slight overestimation in the load-carrying capacity, after yielding in the steel bars of the slab, is attributed to the assumed stiffness of the concrete upon cracking using nonlinear constitutive relationships in the present simulation. The ignoring of the micro cracks for concrete, before testing in the lab and due to the transportation of the culvert sample, in the finite element modeling is another reason for this slight difference between calculated and testing data. The veracity of the finite element analysis was demonstrated as well in the prediction of the crack pattern of culvert at collapse; good agreement was noticed between experimental and numerical analysis observations (Fig. 5). Expected common cracking configuration was seen in the finite element model of the culvert at the location of the maximum bending moments applied on the slab and walls.

james.haido@uod.ac; bashargxabd@gmail.com; ayadaghwan960@gmail.com
michael.dorn@lnu.se; salim.yousif@alqalam.edu.iq

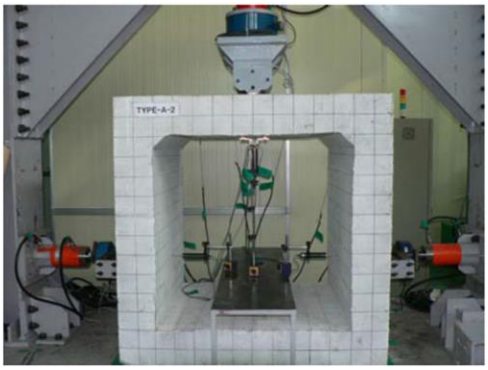

a- Testing setup

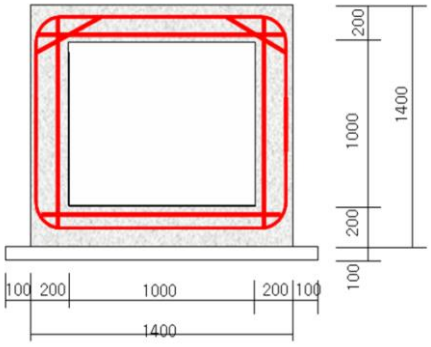

b- Geometry of the culvert

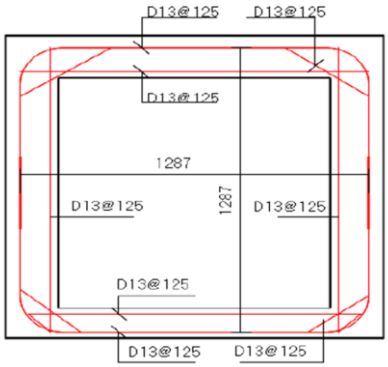

c- Reinforcement of the culvert

Fig. (2): Tested reinforced concrete box culvert [24]

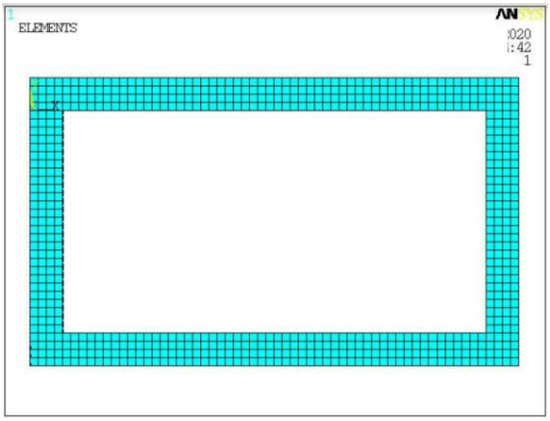

a- Finite element mesh of concrete

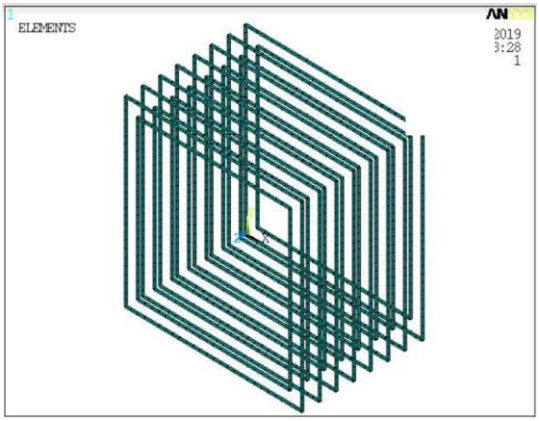

b- Reinforcement bars model

Fig. 3: Finite element mesh of concrete and steel bars of the culvert

james.haido@uod.ac; bashargxabd@gmail.com; ayadaghwan960@gmail.com
michael.dorn@lnu.se; salim.yousif@alqalam.edu.iq

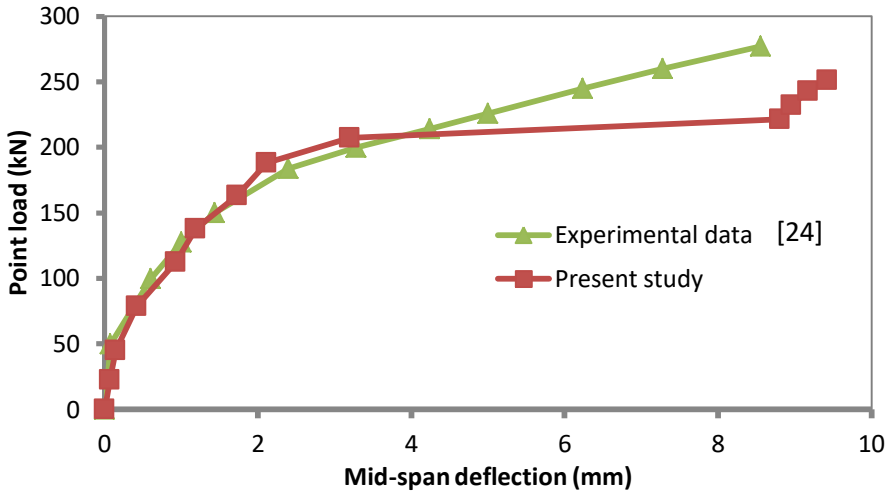

Fig. 4: Structural behavior of the concrete culvert

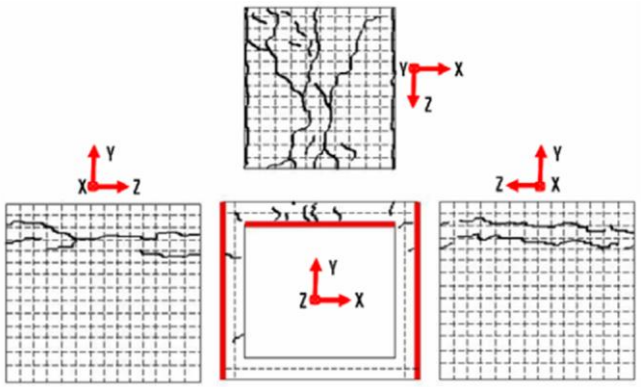

a- experimental observation of cracking [24]

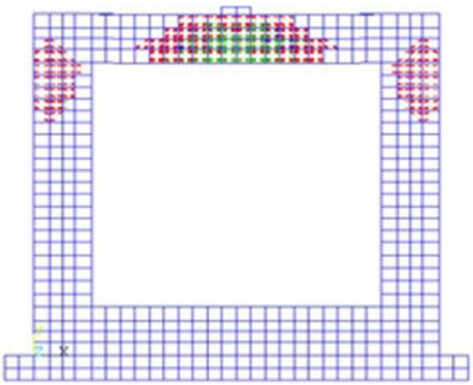

b- Cracking pattern using present finite element modeling

Fig. (5): Cracking pattern of the culvert under applied loading

james.haido@uod.ac; bashargxabd@gmail.com; ayadaghwan960@gmail.com
michael.dorn@lnu.se; salim.yousif@alqalam.edu.iq

4. DEVELOPMENT OF THE ANN PROCEDURE

ANN is an artificial intelligence approach of information processing to mimic how the nerves of the human brain work [25, 26]. This analytical method is configured for specific applications of engineering, viz., prediction of values, data classification and recognition of pattern via learning operation named training of data. The efficiency of an ANN is highly affected by the connection manner of the neurons, the kind of computation that performed by these neurons and way of transmission of pattern for activities throughout the neural network [25]. In this process, an analytical algorithm can be proposed for engineering problems that have complex algorithm solution with conventional analysis techniques. The most widely utilized form of ANNs is a multi-layered network [27] which is simple and depends on using a number of analytical layers of neurons, namely, input, hidden and output layers, that are organized in one strict direction. Each of these layers consists of interconnected neurons or nodes (Fig. 6). These layers are connected by weight values that correlate to the contribution of each input in the predictions. In the present study, a multi-layered feed-forward network with one input layer, one hidden layer and an output layer was used considering the typical configuration of artificial neuron (Fig. 7). This network formulates the approximate solution of nonlinear relationship between inputs (x_i) and outputs (O_j) basing on adjusted weight values. The weights (w_{ij}) are multiplied with the inputs resulted by the neurons. Thereafter, the magnitudes computed from each layer of neurons are transferred by the connections and collected with bias (b_i) as hereunder [25, 27]:

$$O_j = g\left(\sum_{i=1}^{n} w_{ij} x_i + b_i\right) \qquad (2)$$

Eq. 2 is the activation sigmoid function which is adopted in the current work.

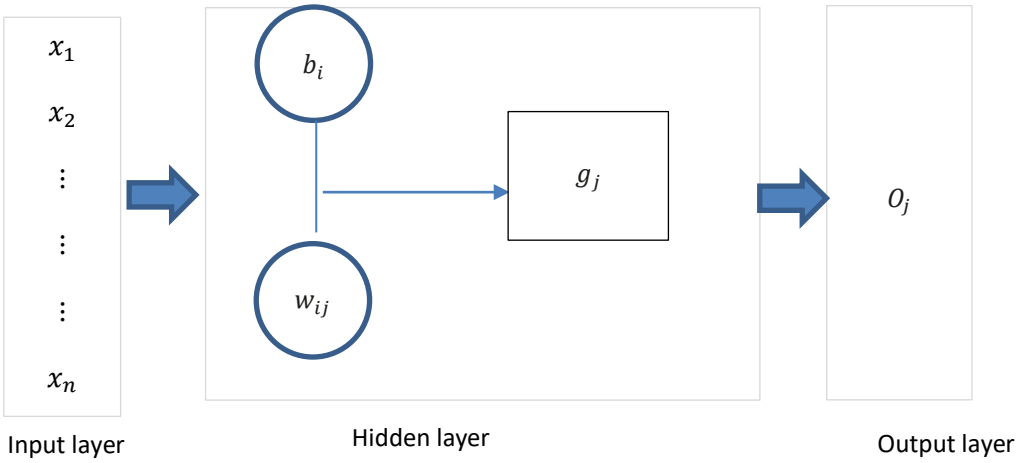

Fig. 6: Typical procedure of the ANN

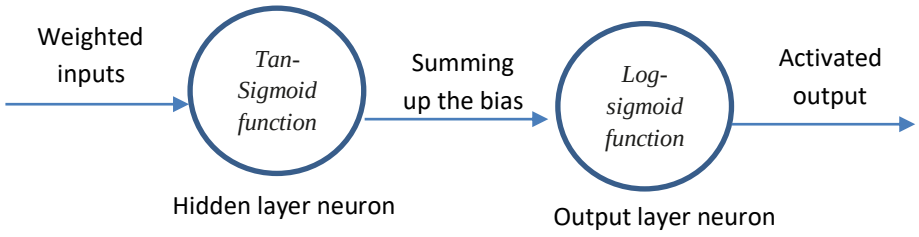

Fig. 7: Typical neuron of ANN

james.haido@uod.ac; bashargxabd@gmail.com; ayadaghwan960@gmail.com
michael.dorn@lnu.se; salim.yousif@alqalam.edu.iq

The database for training of ANN encompasses finite element analysis information for many reinforced concrete box culverts, similar as depicted in Fig 8. The adoption of the input parameters has been relied on their dominant influence on the performance of these structures. The selected inputs in the current ANN are the following: compressive strength of concrete, skew angle of the culvert, thickness of top slab and clear span of the culvert. The width of the walls and their height have only slight influence on the deflection of the top slab and its loading-capacity. Thus, these parameters were kept constant and disregarded in the ANN analysis. Since the structural performance for the concrete culverts is linked to the load-carrying capacity and maximum deflection of the top slab of the culvert, these two values have been employed as target or output data in this study. The load-carrying capacity is given by the maximum concentrated load (F_{max}) applied on the deck or top slab of the culvert and the predicted deformation of the culvert is represented by the maximum mid-span deflection of the top slab.

The validated finite element model was utilized to evaluate a database (Table 1), of ANN, based on the analysis of many box culverts considering different values of the input parameters for neural network. The outputs, in terms of load capacity and maximum deflection, of the finite element analysis of in total 288 skew culverts (Fig. 9) have been used as output database (Table 1) to develop the proposed ANN. The likelihood of divergence and/or numerical instabilities has been minimized during the analysis via normalizing or scaling the input and output data for the ANN. The inputs were scaled between -1 and 1 using the following equation [28]:

$$yi = \frac{2(xi - xi_{max})}{(xi_{max} - xi_{min})} + 1 \quad (3)$$

where,

yi is the scaled value of input

xi is the input value

xi_{min} is the smallest value of xi

xi_{max} is the largest value of xi

The normalization of the output data was performed utilizing a scaling formula as hereunder [28]:

$$yo = \frac{xo - xo_{min}}{xo_{max} - xo_{min}} \quad (4)$$

where,

yo is the scaled value of output ranged 0 and 1

xo is the output value

xo_{min} is the smallest value of xo

xo_{max} is the largest value of xo

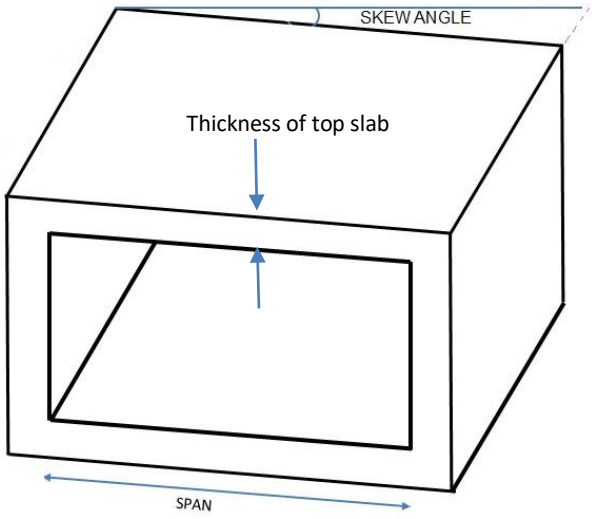

Fig. (8): Schematic representation of the culvert structure investigated

james.haido@uod.ac; bashargxabd@gmail.com; ayadaghwan960@gmail.com
michael.dorn@lnu.se; salim.yousif@alqalam.edu.iq

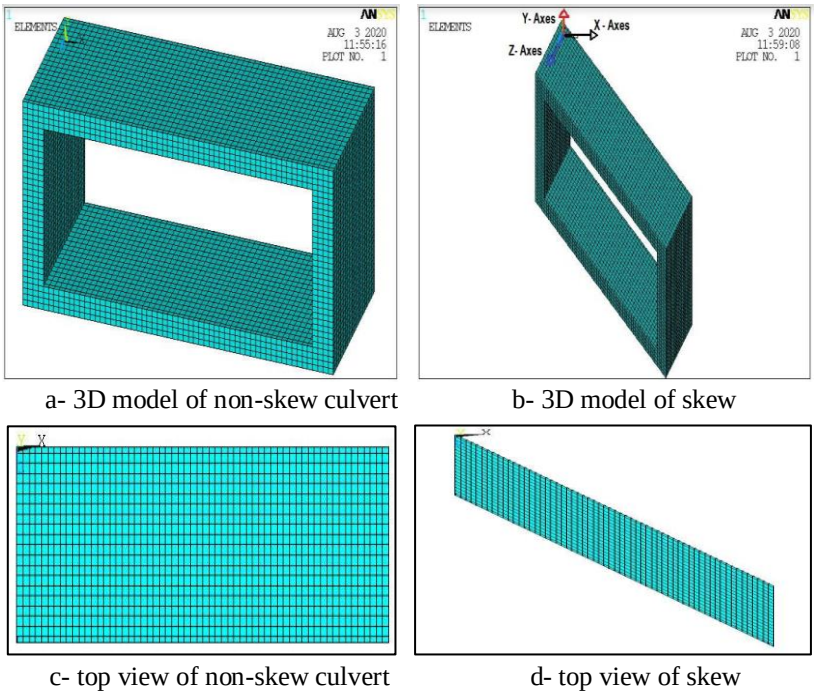

a- 3D model of non-skew culvert b- 3D model of skew

c- top view of non-skew culvert d- top view of skew

Fig. 9: Finite element mesh of the skew culvert model

james.haido@uod.ac; bashargxabd@gmail.com; ayadaghwan960@gmail.com
michael.dorn@lnu.se; salim.yousif@alqalam.edu.iq

Table (1): Database of the present ANN analysis

No.	SPAN (m)	fc' (MPa)	Skew angle (°)	Thickness of slab (mm)	Failure Load (kN)	Deflection (mm)		No.	SPAN (m)	fc' (MPa)	Skew angle (°)	Thickness of slab (mm)	Failure Load (kN)	Deflection (mm)
1	2	20	0	400	3198.9	5.2		49	2	40	0	400	4029.4	10.2
2	2	20	0	300	1917.7	4.5		50	2	40	0	300	1902.9	8.1
3	2	20	0	200	1549.2	3.7		51	2	40	0	200	1534.4	7.3
4	2	20	15	400	2906.3	4.8		52	2	40	15	400	4090.0	8.5
5	2	20	15	300	1976.9	4.1		53	2	40	15	300	1962.2	6.7
6	2	20	15	200	1608.4	3.4		54	2	40	15	200	1593.7	6.0
7	2	20	30	400	2838.3	5.0		55	2	40	30	400	3629.0	5.9
8	2	20	30	300	2036.2	4.1		56	2	40	30	300	2021.4	4.7
9	2	20	30	200	1667.7	3.5		57	2	40	30	200	1652.9	4.2
10	2	20	45	400	2914.0	5.1		58	2	40	45	400	3258.3	8.5
11	2	20	45	300	2095.4	4.1		59	2	40	45	300	2080.7	6.8
12	2	20	45	200	1726.9	3.6		60	2	40	45	200	1712.2	6.1
13	2	26	0	400	3281.0	5.9		61	2	45	0	400	4220.0	9.6
14	2	26	0	300	1913.3	4.7		62	2	45	0	300	1899.2	7.6
15	2	26	0	200	1544.8	4.2		63	2	45	0	200	1530.7	6.8
16	2	26	15	400	3275.5	5.8		64	2	45	15	400	4215.0	8.4
17	2	26	15	300	1972.5	4.7		65	2	45	15	300	1958.5	6.7
18	2	26	15	200	1604.0	4.2		66	2	45	15	200	1590.0	6.0
19	2	26	30	400	2838.3	4.7		67	2	45	30	400	4075.5	7.6
20	2	26	30	300	2031.8	3.7		68	2	45	30	300	2017.7	6.1
21	2	26	30	200	1663.3	3.3		69	2	45	30	200	1649.2	5.4
22	2	26	45	400	2913.0	5.2		70	2	45	45	400	3602.0	6.1
23	2	26	45	300	2091.0	4.2		71	2	45	45	300	2077.0	4.9
24	2	26	45	200	1722.5	3.7		72	2	45	45	200	1708.5	4.4
25	2	30	0	400	3724.0	7.8		73.0	2.0	50.0	0.0	400.0	3872.4	8.1
26	2	30	0	300	1910.3	6.2		74.0	2.0	50.0	0.0	300.0	1895.5	6.5
27	2	30	0	200	1541.8	5.5		75.0	2.0	50.0	0.0	200.0	1527.0	5.8
28	2	30	15	400	3333.8	5.6		76.0	2.0	50.0	15.0	400.0	4300.0	7.3
29	2	30	15	300	1969.6	4.5		77.0	2.0	50.0	15.0	300.0	1954.8	5.8
30	2	30	15	200	1601.1	4.0		78.0	2.0	50.0	15.0	200.0	1586.3	5.2
31	2	30	30	400	3196.0	10.0		79.0	2.0	50.0	30.0	400.0	4293.0	8.6
32	2	30	30	300	2028.8	8.0		80.0	2.0	50.0	30.0	300.0	2014.0	6.8
33	2	30	30	200	1660.3	7.1		81.0	2.0	50.0	30.0	200.0	1645.5	6.1
34	2	30	45	400	2912.0	5.4		82.0	2.0	50.0	45.0	400.0	3835.0	5.8
35	2	30	45	300	2088.1	4.3		83.0	2.0	50.0	45.0	300.0	2073.3	4.6
36	2	30	45	200	1719.6	3.8		84.0	2.0	50.0	45.0	200.0	1704.8	4.1
37	2	35	0	400	3928.5	9.0		85.0	2.0	55.0	0.0	400.0	3836.3	5.9
38	2	35	0	300	1906.6	7.2		86.0	2.0	55.0	0.0	300.0	1891.9	4.7
39	2	35	0	200	1538.1	6.4		87.0	2.0	55.0	0.0	200.0	1523.4	4.2
40	2	35	15	400	3629.0	7.0		88.0	2.0	55.0	15.0	400.0	4700.0	9.4
41	2	35	15	300	1965.9	5.6		89.0	2.0	55.0	15.0	300.0	1951.1	7.4
42	2	35	15	200	1597.4	5.0		90.0	2.0	55.0	15.0	200.0	1582.6	6.7
43	2	35	30	400	3629.0	6.3		91.0	2.0	55.0	30.0	400.0	4493.7	8.2
44	2	35	30	300	2025.1	5.1		92.0	2.0	55.0	30.0	300.0	2010.4	6.5
45	2	35	30	200	1656.6	4.5		93.0	2.0	55.0	30.0	200.0	1641.9	5.9
46	2	35	45	400	3248.4	8.3		94.0	2.0	55.0	45.0	400.0	4046.2	8.3
47	2	35	45	300	2084.4	6.6		95.0	2.0	55.0	45.0	300.0	2069.6	6.6
48	2	35	45	200	1715.9	5.9		96.0	2.0	55.0	45.0	200.0	1701.1	5.9

james.haido@uod.ac; bashargxabd@gmail.com; ayadaghwan960@gmail.com
michael.dorn@lnu.se; salim.yousif@alqalam.edu.iq

Table 1: continued

No.	SPAN (m)	fc' (MPa)	Skew angle (°)	Thickness of slab (mm)	Failure Load (kN)	Deflection (mm)		No.	SPAN (m)	fc' (MPa)	Skew angle (°)	Thickness of slab (mm)	Failure Load (kN)	Deflection (mm)
97	4	20	0	400	1173.38	18.81016		145	4	40	0	400	1203.0	33.5
98	4	20	0	300	1021.61	14.98437		146	4	40	0	300	1006.8	26.6
99	4	20	0	200	653.108	13.39029		147	4	40	0	200	638.3	23.8
100	4	20	15	400	1124.19	15.79333		148	4	40	15	400	1323.0	33.0
101	4	20	15	300	1080.86	12.58113		149	4	40	15	300	1066.1	26.3
102	4	20	15	200	712.358	11.24271		150	4	40	15	200	697.6	23.5
103	4	20	30	400	931.384	9.221564		151	4	40	30	400	1354.5	26.9
104	4	20	30	300	1140.11	7.345992		152	4	40	30	300	1125.3	21.4
105	4	20	30	200	771.608	6.564503		153	4	40	30	200	756.8	19.1
106	4	20	45	400	916.719	28.91565		154	4	40	45	400	1194.4	25.3
107	4	20	45	300	1199.36	23.0345		155	4	40	45	300	1184.6	20.2
108	4	20	45	200	830.858	20.58402		156	4	40	45	200	816.1	18.0
109	4	26	0	400	1173.38	24.2		157	4	45	0	400	1203.0	22.0
110	4	26	0	300	1017.18	19.27797		158	4	45	0	300	1003.2	17.5
111	4	26	0	200	648.68	17.22712		159	4	45	0	200	634.7	15.7
112	4	26	15	400	1204.88	22		160	4	45	15	400	1323.0	33.0
113	4	26	15	300	1076.43	17.52542		161	4	45	15	300	1062.4	26.3
114	4	26	15	200	707.93	15.66102		162	4	45	15	200	693.9	23.5
115	4	26	30	400	1038	12.3		163	4	45	30	400	1462.5	23.0
116	4	26	30	300	1135.68	9.798305		164	4	45	30	300	1121.7	18.3
117	4	26	30	200	767.18	8.755932		165	4	45	30	200	753.2	16.4
118	4	26	45	400	979.125	24.2		166	4	45	45	400	1236.3	26.0
119	4	26	45	300	1194.93	19.27797		167	4	45	45	300	1180.9	20.7
120	4	26	45	200	826.43	17.22712		168	4	45	45	200	812.4	18.5
121	4	30	0	400	1177.31	19.4		169	4	50	0	400	1203.0	21.3
122	4	30	0	300	1014.23	15.45424		170	4	50	0	300	999.5	17.0
123	4	30	0	200	645.728	13.81017		171	4	50	0	200	631.0	15.2
124	4	30	15	400	1239.8	20.55		172	4	50	15	400	1348.6	28.3
125	4	30	15	300	1073.48	16.37034		173	4	50	15	300	1058.7	22.5
126	4	30	15	200	704.978	14.62881		174	4	50	15	200	690.2	20.1
127	4	30	30	400	1118.25	17.15		175	4	50	30	400	1488.0	40.7
128	4	30	30	300	1132.73	13.66186		176	4	50	30	300	1118.0	32.4
129	4	30	30	200	764.228	12.20847		177	4	50	30	200	749.5	29.0
130	4	30	45	400	1017.2	22		178	4	50	45	400	1445.4	34.8
131	4	30	45	300	1191.98	17.52542		179	4	50	45	300	1177.2	27.7
132	4	30	45	200	823.478	15.66102		180	4	50	45	200	808.7	24.8
133	4	35	0	400	1203	26		181	4	55	0	400	1260.0	38.4
134	4	35	0	300	1010.54	20.71186		182	4	55	0	300	995.8	30.6
135	4	35	0	200	642.038	18.50847		183	4	55	0	200	627.3	27.3
136	4	35	15	400	1234.4	23.69		184	4	55	15	400	1380.0	29.0
137	4	35	15	300	1069.79	18.87169		185	4	55	15	300	1055.0	23.1
138	4	35	15	200	701.288	16.86407		186	4	55	15	200	686.5	20.6
139	4	35	30	400	1215.38	20.13		187	4	55	30	400	1459.0	40.5
140	4	35	30	300	1129.04	16.03576		188	4	55	30	300	1114.3	33.4
141	4	35	30	200	760.538	14.32983		189	4	55	30	200	745.8	28.8
142	4	35	45	400	1118.25	30.23		190	4	55	45	400	1543.0	45.4
143	4	35	45	300	1188.29	24.08153		191	4	55	45	300	1173.5	36.1
144	4	35	45	200	819.788	21.51966		192	4	55	45	200	805.0	32.3

james.haido@uod.ac; bashargxabd@gmail.com; ayadaghwan960@gmail.com
michael.dorn@lnu.se; salim.yousif@alqalam.edu.iq

Table 1: continued

No.	SPAN (m)	fc' (MPa)	Skew angle (°)	Thickness of slab (mm)	Failure Load (kN)	Deflection (mm)		No.	SPAN (m)	fc' (MPa)	Skew angle (°)	Thickness of slab (mm)	Failure Load (kN)	Deflection (mm)
193	6	20	0	400	666.4	28.5		241.0	6.0	40.0	0.0	400.0	721.9	75.4
194	6	20	0	300	125.5	22.7		242.0	6.0	40.0	0.0	300.0	110.8	60.1
195	6	20	0	200	24.0	20.3		243.0	6.0	40.0	0.0	200.0	17.0	53.7
196	6	20	15	400	703.5	55.6		244.0	6.0	40.0	15.0	400.0	763.9	50.3
197	6	20	15	300	184.8	44.3		245.0	6.0	40.0	15.0	300.0	170.0	40.1
198	6	20	15	200	48.0	39.6		246.0	6.0	40.0	15.0	200.0	37.8	35.8
199	6	20	30	400	590.6	31.2		247.0	6.0	40.0	30.0	400.0	785.9	39.2
200	6	20	30	300	244.0	24.9		248.0	6.0	40.0	30.0	300.0	229.3	31.2
201	6	20	30	200	100.0	22.2		249.0	6.0	40.0	30.0	200.0	66.9	27.9
202	6	20	45	400	515.5	26.0		250.0	6.0	40.0	45.0	400.0	664.1	56.0
203	6	20	45	300	303.3	20.7		251.0	6.0	40.0	45.0	300.0	288.5	44.6
204	6	20	45	200	91.1	18.5		252.0	6.0	40.0	45.0	200.0	125.3	39.9
205	6	26	0	400	682.5	42.0		253.0	6.0	45.0	0.0	400.0	722.0	80.0
206	6	26	0	300	121.1	33.5		254.0	6.0	45.0	0.0	300.0	107.1	63.7
207	6	26	0	200	21.8	29.9		255.0	6.0	45.0	0.0	200.0	15.9	56.9
208	6	26	15	400	703.5	42.0		256.0	6.0	45.0	15.0	400.0	781.0	59.0
209	6	26	15	300	180.4	33.5		257.0	6.0	45.0	15.0	300.0	166.3	47.0
210	6	26	15	200	46.2	29.9		258.0	6.0	45.0	15.0	200.0	35.4	42.0
211	6	26	30	400	624.8	27.5		259.0	6.0	45.0	30.0	400.0	840.0	81.5
212	6	26	30	300	239.6	21.9		260.0	6.0	45.0	30.0	300.0	225.6	64.9
213	6	26	30	200	91.9	19.5		261.0	6.0	45.0	30.0	200.0	60.6	58.0
214	6	26	45	400	567.0	36.4		262.0	6.0	45.0	45.0	400.0	703.5	57.0
215	6	26	45	300	298.9	29.0		263.0	6.0	45.0	45.0	300.0	284.8	45.4
216	6	26	45	200	157.5	25.9		264.0	6.0	45.0	45.0	200.0	115.3	40.6
217.0	6.0	30.0	0.0	400.0	721.9	46.5		265.0	6.0	50.0	0.0	400.0	722.0	53.0
218.0	6.0	30.0	0.0	300.0	118.1	37.1		266.0	6.0	50.0	0.0	300.0	103.4	42.2
219.0	6.0	30.0	0.0	200.0	19.3	33.1		267.0	6.0	50.0	0.0	200.0	14.8	37.7
220.0	6.0	30.0	15.0	400.0	721.9	40.3		268.0	6.0	50.0	15.0	400.0	866.3	76.3
221.0	6.0	30.0	15.0	300.0	177.4	32.1		269.0	6.0	50.0	15.0	300.0	162.6	60.8
222.0	6.0	30.0	15.0	200.0	43.6	28.7		270.0	6.0	50.0	15.0	200.0	30.5	54.3
223.0	6.0	30.0	30.0	400.0	664.1	33.6		271.0	6.0	50.0	30.0	400.0	657.6	22.0
224.0	6.0	30.0	30.0	300.0	236.6	26.8		272.0	6.0	50.0	30.0	300.0	221.9	17.5
225.0	6.0	30.0	30.0	200.0	84.3	23.9		273.0	6.0	50.0	30.0	200.0	74.9	15.7
226.0	6.0	30.0	45.0	400.0	525.0	30.0		274.0	6.0	50.0	45.0	400.0	721.9	57.7
227.0	6.0	30.0	45.0	300.0	295.9	23.9		275.0	6.0	50.0	45.0	300.0	281.1	46.0
228.0	6.0	30.0	45.0	200.0	166.8	21.4		276.0	6.0	50.0	45.0	200.0	109.5	41.1
229.0	6.0	35.0	0.0	400.0	704.9	51.2		277.0	6.0	55.0	0.0	400.0	721.8	58.5
230.0	6.0	35.0	0.0	300.0	114.5	40.8		278.0	6.0	55.0	0.0	300.0	99.7	46.6
231.0	6.0	35.0	0.0	200.0	18.6	36.4		279.0	6.0	55.0	0.0	200.0	13.8	41.6
232.0	6.0	35.0	15.0	400.0	763.9	66.6		280.0	6.0	55.0	15.0	400.0	781.0	45.6
233.0	6.0	35.0	15.0	300.0	173.7	53.1		281.0	6.0	55.0	15.0	300.0	158.9	36.3
234.0	6.0	35.0	15.0	200.0	39.5	47.4		282.0	6.0	55.0	15.0	200.0	32.3	32.5
235.0	6.0	35.0	30.0	400.0	742.9	44.6		283.0	6.0	55.0	30.0	400.0	764.0	42.0
236.0	6.0	35.0	30.0	300.0	233.0	35.5		284.0	6.0	55.0	30.0	300.0	218.2	33.5
237.0	6.0	35.0	30.0	200.0	73.1	31.7		285.0	6.0	55.0	30.0	200.0	62.3	29.9
238.0	6.0	35.0	45.0	400.0	603.8	40.0		286.0	6.0	55.0	45.0	400.0	742.8	54.2
239.0	6.0	35.0	45.0	300.0	292.2	31.9		287.0	6.0	55.0	45.0	300.0	277.4	43.2
240.0	6.0	35.0	45.0	200.0	141.4	28.5		288.0	6.0	55.0	45.0	200.0	103.6	38.6

james.haido@uod.ac; bashargxabd@gmail.com; ayadaghwan960@gmail.com
michael.dorn@lnu.se; salim.yousif@alqalam.edu.iq

The input layer of the current network comprises of four neurons depending on their expected remarkable effect on the structural performance of the culvert. These neurons are consisting of four parameters, namely, the clear span of the top slab of culvert, its skew angle, thickness of the top slab and the compressive strength of concrete. Throughout the training of the ANN, a number of its architecture was checked via changing the neuron number per hidden layer to achieve the appropriate and stable neural model. Two forms of the activation functions were employed in this regard, namely, first Tan-sigmoid and Log-sigmoid functions for hidden and output layers. Accordingly, one layer has been adopted as a hidden layer concerned with the use of neural network for predicting the outputs of concrete culverts and it was demonstrated that the use of 3 neurons for hidden layer results converged predictions. The architecture of the present ANN procedure regarding the output layer is comprising a single neuron, which is either the maximum deflection of the top slab or its transverse loading capacity. In view of that mentioned above, the proposed ANN algorithms adopted in the current work are two models with the same number of neuron layers as depicted in Fig 10. The training process of the ANN data covers tuning the magnitudes of the biases and weights that are randomly assigned at first to reach the optimized performance of the network depending on the iterative manner. The default error (Eq. 5) [25, 27] or difference between the outputs and their target data refers to the efficiency of the feed-forward ANN.

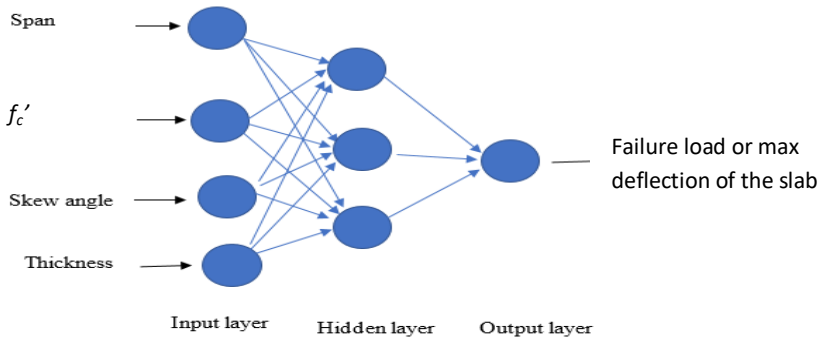

Fig. 910): Architecture of the present ANN

$$Error\% = \frac{1}{n}\sum_{i=1}^{n}(t_i - y_i) \qquad (5)$$

where, t_i and y_i are the target or desired output and predicted values of ANN, respectively.

The back-propagation error was employed in this study to minimize the error encountered at output nodes during each iteration. Hence, a smaller error was achieved throughout this approach by readjusting of weight and bias of the ANN analysis. In addition, the accuracy of the present ANN predictions was improved via dividing the normalized data of inputs and target data into training, validation and testing data. The Levenberg-Marquardt (LM) method [28-30] is a training function based on the conjugate gradient algorithms. This function was adopted in the present neural network analysis due to that it is faster than traditional descent-type methods of data training. In the current study, 80% of the input and target data were used in training process, 10% of them in validation and 10% of data for testing purpose. The algorithms of the ANN are sorted as local and global types; the local strategies are preferred in the analysis due to their relation to ANN concept in distribution process of data [25, 31]. Moreover, the target outputs are achieved faster using local algorithms; where the computational prediction is carried out independently [31]. The local algorithm of ANN was chosen in the present study with deterministic nature. This process involves an iterative operation, for data, which is repeated until meeting one of the solving conditions listed in Table 2. The flowchart of the current learning ANN algorithm coded in MATLAB is shown in Fig 11.

james.haido@uod.ac; bashargxabd@gmail.com; ayadaghwan960@gmail.com
michael.dorn@lnu.se; salim.yousif@alqalam.edu.iq

Table 2: Conditions of the iterative process for the present ANN

Conditional item	Value
Maximum number of iterations or epochs of training	1000
Performance goal value of ANN to measure the difference between he output and target values	0.0
Minimum gradient of the performance of present ANN	10^{-7}

5. THE PROPOSED ANN MODELS

The two ANN procedures inspected have been utilized to formulate simple mathematical expressions to predict both the load-carrying capacity of the culvert and the maximum deflection of its top slab. The superiority of these developed expressions was assessed via comparing the computed values of these two outputs with 288 finite element results listed in Table 1. The database for the load-carrying capacity (failure load) and the maximum deflection of top slab of culvert were used to establish ANN procedure for predicting this load. A proper correlation coefficient greater than 90% was obtained for these two parameters during the process of training, validation and testing of data as depicted in Figs 12 and 13. More specifically, slight divergence was observed between the predicted and actual magnitudes of the outputs based on the training, validation and testing processes of the data. The error, between the target values from the finite element analysis and the ANN outputs (Figs 14 and 15) for failure load and maximum deflection, also confirms the validation of the presented ANN algorithm, where the trivial error was noticed in calculation using only 25 epochs or iterations. Accordingly, an average small error was achieved with approximate coinciding with zero error line accompanying with large frequency of the training, validation and testing data. The contribution of each input in the prediction of the load-carrying capacity and maximum deflection of the top slab of the culvert, was investigated in terms of the importance percentage as shown in Figs 16 and 17. Outcomes reveal that the skew angle has slight effect on the load capacity of the culvert and maximum deflection of its slab due to the semi-constant behavior of the top slab with increasing in skew angle at the largest spans of this slab. Furthermore, geometry of the top slab of the culvert shows high influence on the outputs of the ANN. Aforementioned functions for each ANN layer were applied in the formulation of simple equation to predict the failure load of the culvert and its top slab deformation depended on the importance of each inputs as follows:

$$yi1 = 0.5(L - 6) + 1 \quad (6)$$

$$yi2 = 0.0571(f'c - 55) + 1 \quad (7)$$

$$yi3 = 0.0444(\theta - 45) + 1 \quad (8)$$

$$yi4 = 0.01(t - 400) + 1 \quad (9)$$

$$X1 = -9.7569 + 9.5383yi1 + 0.1132yi2 - 0.07337yi3 - 0.7872yi4 \quad \text{for failure load model} \quad (10)$$

$$X2 = -2.8082 - 1.2304yi1 + 0.0681yi2 - 0.0268yi3 + 0.3678yi4 \quad \text{for failure load model} \quad (11)$$

$$X3 = 4.5220 - 0.07836yi1 - 3.9728yi2 + 0.6393yi3 - 4.7327yi4 \quad \text{for failure load model} \quad (12)$$

$$X1 = 0.1827 + 0.4283yi1 + 0.1220yi2 - 0.0577yi3 + 0.0839yi4 \quad \text{for deflection model} \quad (13)$$

$$X2 = 0.6041 - 5.0627yi1 - 0.3092yi2 + 0.7767yi3 - 0.3690yi4 \quad \text{for deflection model} \quad (14)$$

james.haido@uod.ac; bashargxabd@gmail.com; ayadaghwan960@gmail.com
michael.dorn@lnu.se; salim.yousif@alqalam.edu.iq

$X3 = -3.8050 - 2.3972yi1 - 0.4350yi2 - 0.3900yi3 - 1.6350yi4$ for deflection model (15)

$$XX1 = \frac{2}{1+e^{-2X1}} - 1 \quad (16)$$

$$XX2 = \frac{2}{1+e^{-2X2}} - 1 \quad (17)$$

$$XX3 = \frac{2}{1+e^{-2X3}} - 1 \quad (18)$$

$XX = 11.7910 - 2.2059XX1 + 15.2457XX2 - 0.2100XX3$ for failure load model (19)

$XX = -3.3993 + 6.0904XX1 + 0.7232XX2 - 0.7276XX3$ for deflection model (20)

$$X = \frac{1}{1+e^{-XX}} \quad (21)$$

$Failure\ Load\ (kN) = 13.8 + 4686.2X$ (22)

$deflection\ (mm) = 3.3 + 78.2X$ (23)

Where *yi1*, *yi2*,*yi3* and *yi4* are normalized input
X1, *X2and X3* are weighted inputs for hidden layer
XX1, *XX2* and *XX3* are activation functions for hidden layer
XX is weighted input for output layer
X is activation function for output layer

james.haido@uod.ac; bashargxabd@gmail.com; ayadaghwan960@gmail.com
michael.dorn@lnu.se; salim.yousif@alqalam.edu.iq

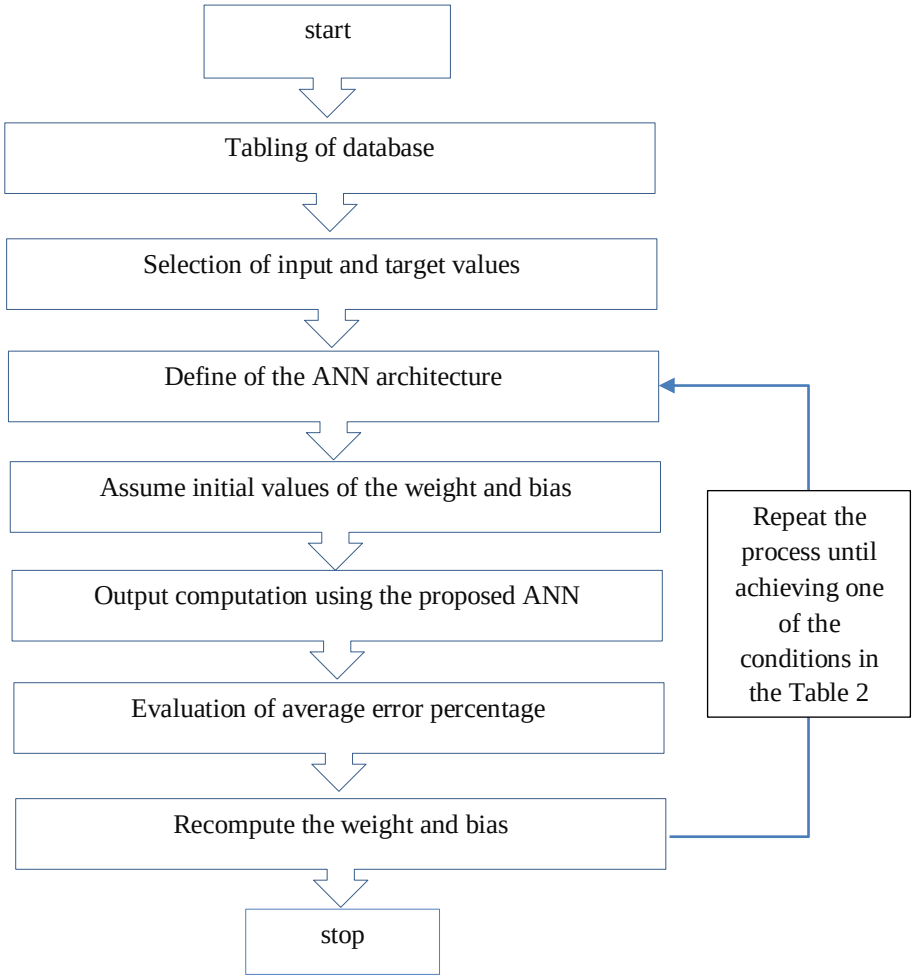

Fig. (11): Iterative process of the present ANN model

james.haido@uod.ac; bashargxabd@gmail.com; ayadaghwan960@gmail.com
michael.dorn@lnu.se; salim.yousif@alqalam.edu.iq

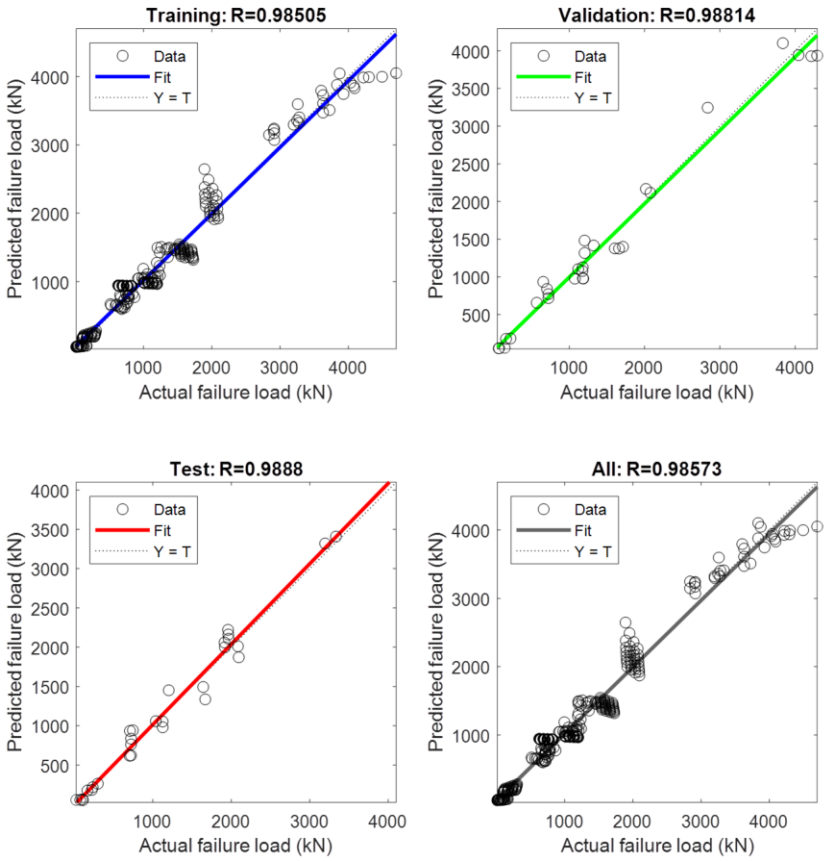

Note: R is the correlation coefficient, Y is the ANN prediction, and T is the target value.

Fig. (12): Correlation between ANN predicted and target data of failure load

james.haido@uod.ac; bashargxabd@gmail.com; ayadaghwan960@gmail.com
michael.dorn@lnu.se; salim.yousif@alqalam.edu.iq

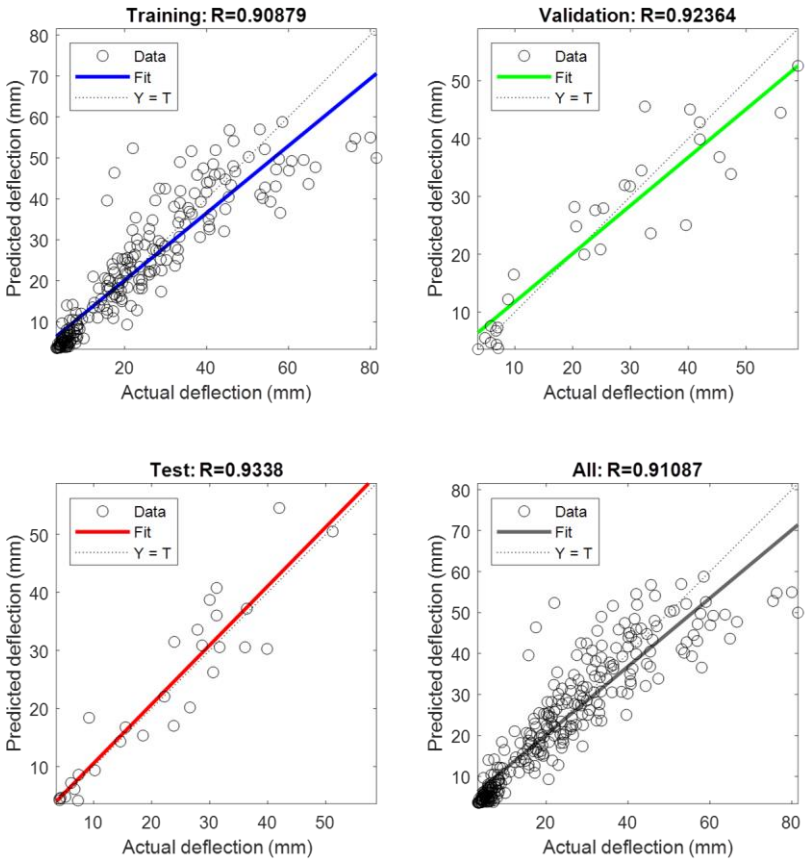

Fig. (13): Correlation between ANN predicted and target data of maximum deflection

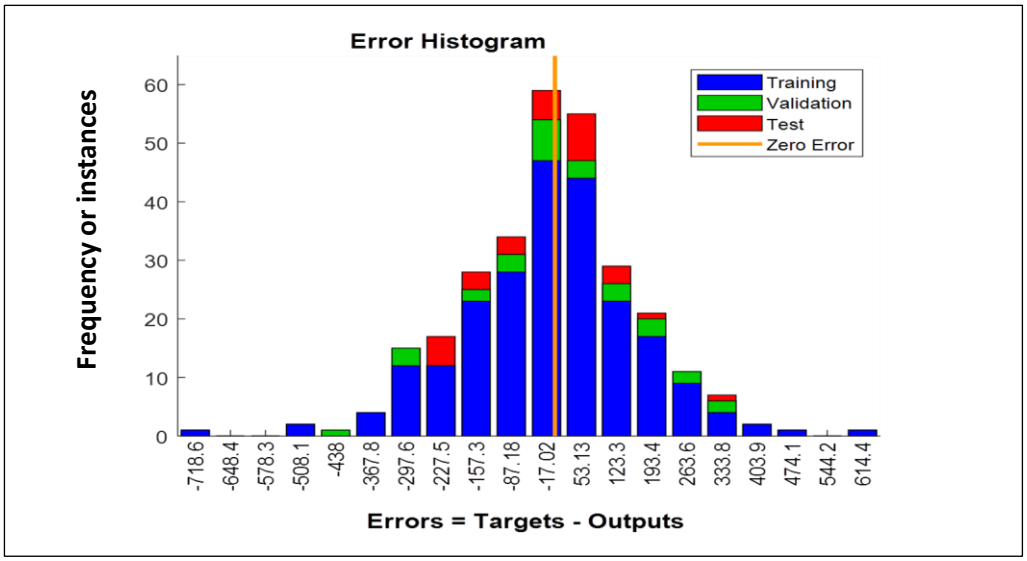

Fig. 15: Error histogram of the predicted maximum deflection

james.haido@uod.ac; bashargxabd@gmail.com; ayadaghwan960@gmail.com
michael.dorn@lnu.se; salim.yousif@alqalam.edu.iq

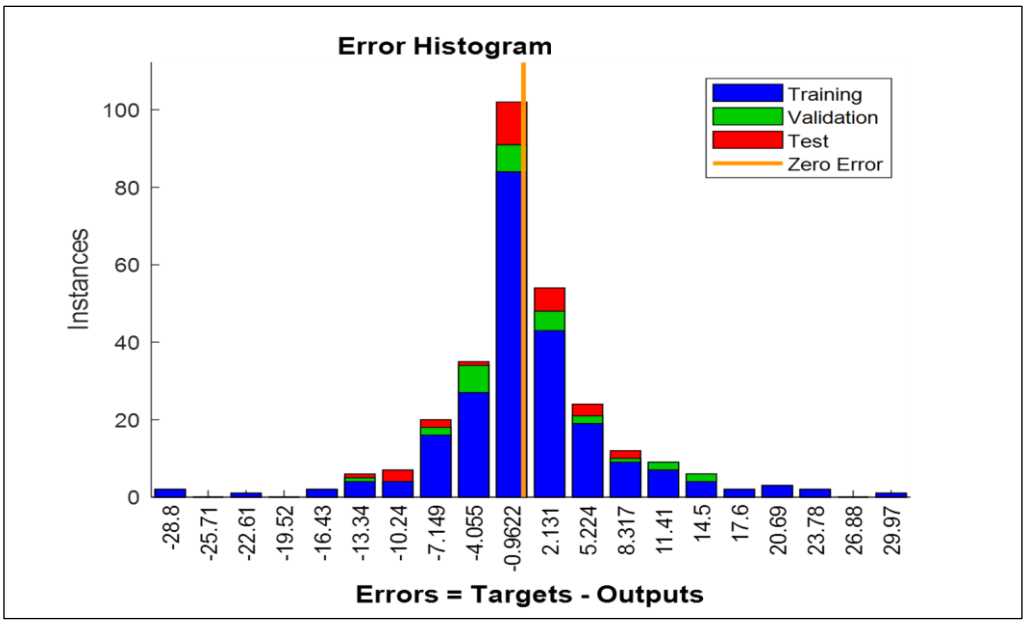

Fig. 16: Importance of the inputs for failure load model

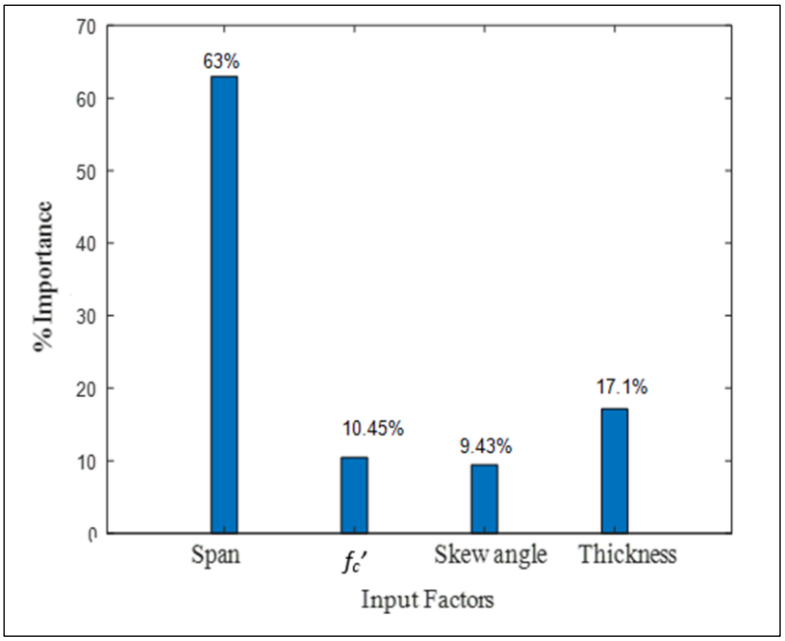

Fig. 17: Importance of the inputs for maximum deflection model

6. CONCLUSIONS

In the present study, the validation of particular constitutive models for the behavior of concrete and steel bars has been investigated in the simulation of the performance of reinforced concrete single cell box culvert. In addition, artificial neural network models have been developed in MATLAB to predict load-carrying capacity and maximum deflection of the top slab of this structures based on a parametric study for analysis of 288 skew culverts using current finite element analysis. Accordingly, simple equations have been formulated depending on the ANN outcomes to compute these two outputs of the skew culvert utilizing its concrete compressive strength, clear span of the top slab, thickness of the top slab and skew angle as independent input parameters. The analysis of error, between the outputs of finite element simulation and ANN outcomes, demonstrates the consideration of these input parameters in ANN analysis

james.haido@uod.ac; bashargxabd@gmail.com; ayadaghwan960@gmail.com
michael.dorn@lnu.se; salim.yousif@alqalam.edu.iq

especially the span of the slab and its thickness that significantly contribute in the improvement of the reliability of the proposed ANN models. In contrast with the tedious finite element modeling, the proposed ANN equations, for determining failure load and maximum deformation of the top slab for concrete culvert, perform well in terms of simplicity in predicating the load-carrying capacity of this structure and its top slab deflection.

REFERENCES

Najafi M, Bhattachar DV. Development of a culvert inventory and inspection framework for asset management of road structures. Journal of King Saud University – Science 2011; 23: 243–254.

Chen B, Sun L. Performance of a Reinforced Concrete Box Culvert Installed in Trapezoidal Trenches. J. Bridge Eng. 2014; 19: 120-130

Dasgupta A, Sengupta B. Large-Scale M od el T est on Square B ox Culvert Backfilled with Sand. J. Geotech. Engrg. 1991; 117: 156-161.

Scanlon R. F. Detailed visual culvert inspection guidelines (Level 2 Inspections), Main Road, Weastern Australia, 2010.

Department of Transportation – USA. Reinforced Concrete Box Culverts and Similar Structures, Chapter in the Highway Design Manual, 2020.

Katona MG, Vittes PD. Soil-structure analysis and evaluation of buried box-culvert designs. Transport Res Rec Transport Res Board 1982; 878:1–7 [Washington, DC].

Kim K, Yoo CH. Design loading on deeply buried box culverts. J Geotech Geoenviron Eng – ASCE 2005;131(1):20–7.

Abuhajar O, El Naggar H, Newson T. Static soil culvert interaction the effect of box culvert geometric configurations and soil properties. Computers and Geotechnics 2015; 69: 219–235.

Chauhuan VD, Solanki G, Tressa M. Analysis of Box Type Multi-Barrel Skew Culvert. Journal of Emerging. Technologies and Innovative Research 2018; 5 (4)

Zoghi M, Farhey DN, Gawandi A. Influence of Haunches on Performance of Precast-Concrete, Short-Span, Skewed Bridges with Integral Abutment Walls. J. Perform. Constr. Facil. 2008; 22: 101-107.

Kim K, Yoo CH. Design loading on deeply buried box culverts. J Geotech Geoenviron Eng 2005;131(1):20–7.

Tao Q, He Z, Jia Y. Influence of flling properties and culvert structure parameters on the soil arching effect of upper-buried-type culverts. Results in Physics 2020; 16.

Yatsumoto H, Mitsuyoshi Y, Sawamura Y, Kimura M. Evaluation of seismic behavior of box culvert buried in the ground through centrifuge model tests and numerical analysis. Underground space 2019; 4: 147-167.

Bennett RM, Wood SM, Drumm EC, Rainwater NR. Vertical loads on concrete box culverts under high embankments. J Bridge Eng – ASCE 2005;10(6):643–9.

Kang J, Parker F, Kang YJ, Yoo CH. Effects of frictional forces acting on sidewalls of buried box culverts. Int J Numer Anal Methods 2008;32(3):289–306.

McGuigan BL, Valsangkar AJ. Centrifuge testing and numerical analysis of box culverts installed in induced trenches. Can Geotech J 2010;47(2):147–63.

Pimentel M, Costa P, Félix C, Figueiras J. Behavior of reinforced concrete box culverts under high embankments. J Struct Eng – ASCE 2009;135(4):366–75.

Yeom SM, Seong JH, Yu Y, Soo SD, Hoon LJ,Hoon JJ. Optimal Joint Position in Concrete Pavement Slab over Skewed Box Culvert. Int. J. Highw. Eng 2013;15(5): 47-55

Kumar VR, Ingle RK. Finite Element Analysis of Skew Box Underpass Bridge – few observations. Indian Highways 2016; 44 (20):

SS-EN 1992-1-1:2005, Eurocode 2: Design of concrete structures - Part 1 - 1: General rules

james.haido@uod.ac; bashargxabd@gmail.com; ayadaghwan960@gmail.com
michael.dorn@lnu.se; salim.yousif@alqalam.edu.iq

and rules for buildings, Stockholm: SIS, Swedish Standard Institute, 2005.

American Concrete Institute Committee (ACI 318-14 committee), Building Code Requirements for Structural Concrete, 2014.

ANSYS, Inc., ANSYS Manual - Release 11.0, Documentation, 2007.

Si Gao, Tiegang Liu, Chengbao Yao, A complete list of exact solutions for one-dimensional elastic-perfectly plastic solid Riemann problem without vacuum, Communications in Nonlinear Science and Numerical Simulation, 63, 2018.

Woo S.K., Jo J.H., Kwon Y.G. Failure behavior characteristics of box culvert using 3-Axes loading. Fracture Mechanics of Concrete and Concrete Structures - High Performance, Fiber Reinforced Concrete, Special Loadings and Structural Applications- B. H. Oh, et al., Korea Concrete Institute, 2010.

Gregoria M. Kotsovou, Demitrios M. Cotsovos, Nikos D. Lagaros, Assessment of RC exterior beam-column Joints based on artificial neural networks and other methods, Engineering Structures, 144, 2017.

Yousif ST, Abdul-Razzak AA. Artificial neural networks model for predicting nonlinear response of rectangular plates. International Conference on Innovative and Smart Structural Systems for Sustainable Habitat (INSHAB-2008). Coimbatore, India, 2008.

Abdul-Razzak AA., Yousif ST. Artificial Neural Network Model for Predicting Nonlinear Response of Uniformly Loaded Fixed Plates. Eng. & Technology, Vol.25, No.3, 2007.

Yousif ST, Abdul-Razzak AA. Artificial Neural Networks Modeling of Elasto-Plastic Plates. Scholar's Press Publisher, Germany, 2017.

Yousif ST, Abdul-Razzak AA. Analysis of Elasto-Plastic Plates using Artificial Neural Networks, Published in (Proc. of the Ninth Inter. Conf. on the Appli. of Artificial Intelligence to Civil, Structural and Environmental Engineering), St. Julians, Malta, 18-21 Sept. 2007.

Howard, D., and Mark, B., Deep learning toolbox, User's Guide, R2020a. the Math works, Inc., 2020.

Lagaros ND, Papadrakakis M. Improving the condition of the Jacobian in neural network training. Adv Eng Software 2004;35(1):9–25.

james.haido@uod.ac; bashargxabd@gmail.com; ayadaghwan960@gmail.com
michael.dorn@lnu.se; salim.yousif@alqalam.edu.iq